MODELING OF MECHANICAL PROPERTIES OF MULTI-LAYERED PILLARED GRAPHENE NANOSTRUCTURES

S. Sihn[1,2]*, V. Varshney[1,3], A. K. Roy[1], B. L. Farmer[1]
[1] Air Force Research Laboratory, Materials and Manufacturing Directorate, AFRL/RXBT, Wright-Patterson Air Force Base, OH 45433, USA,
[2] University of Dayton Research Institute, Multi-Scale Composites and Polymer Division, 300 College Park, Dayton, OH 45469-0060, USA,
[3] Universal Technology Corporation, 1270 N. Fairfield Rd., Dayton, OH 45432, USA
* Corresponding author (sangwook@stanfordalumni.org)

Keywords: *Pillared graphene structure, graphene, carbon nanotube, structure molecular mechanics method.*

Abstract

A computational finite element analysis-based structural molecular mechanics was conducted to predict effective mechanical properties of a 3-D novel carbon structure, multi-layered pillared graphene nanostructure (mPGS), which is constituted with several multi-layered graphene sheets and multi-walled carbon nanotubes as pillars. Various representative unitcell models were developed for predicting the mechanical properties of the mPGSs having different values of pillar length and inter-pillar distance. Proper selections of the periodic geometry and boundary conditions enable the unitcell model to yield consistent results with minimal size and edge effects. The simulation results show that the mPGS yields significantly improved effective Young's and shear moduli compared with the single-layered PGS, especially the out-of-plane Young's and shear moduli. A parametric study shows that the pillar length and inter-pillar distance significantly affect the 3-D effective in-plane and through-thickness properties. The mPGS possesses negative in-plane Poisson's ratios regardless of its dimension.

1. Introduction

Carbon nanotubes (CNTs) and graphite (as well as graphene) are often given special attention because of their excellent multifunctional properties that include thermal and electrical conductivity, as well as mechanical stiffness and strength. It should be noted that these CNT and graphite/graphene are inherently considered as 1-D and 2-D structures, respectively, which result in their anisotropic material properties. For example, it is well known that the graphite possesses excellent tensile modulus and strength in the planar directions due to strong C-C covalent bonding, but weak shear properties because of the poor van der Waals interactions between the graphene sheets. Multi-walled CNTs and CNT bundles are known to have weak shear properties due to the same reason. One of the ways to tailor the anisotropy is to develop 3-dimensional carbon-based network structures.

One of such novel carbon-based architectures comprising of the nanotubes and graphene sheets is a pillared graphene structure (PGS), which was first reported by Dimitrakakis, et al. [1] in context of its enhanced hydrogen storage capability. Despite of premature stage, some experimental work has already been pursued to fabricate and characterize the PGS [2, 3]. Meanwhile, several simulation efforts have been reported to predict thermal [4] and electronic [5] transport behaviors of the PGS using atomistic molecular dynamics (MD) and first-principle simulations, respectively.

Because of its column-like CNT network, the static, dynamic and buckling behaviors of the PGS could significantly depend on the geometric parameters, including the pillar length and inter-pillar distance, as well as defects and imperfections at the junction. Therefore, it is crucial to assess its structural performance in order to utilize it as a multifunctional material.

Because of huge computational tasks, practical applications of the atomistic modeling techniques, such as classical MD, tight binding molecular dynamics (TBMD), density functional theory (DFT), etc., are often limited by system size, and are usually confined to studies of relatively "short-term" phenomena at the timescales from a few femtoseconds (TBMD) to a few nanoseconds (classical MD). On the other hand, a classical continuum mechanics approach using shell models or solid models can handle relatively large system size problems for "long-term" phenomenon, but could sacrifice accuracy by losing atomistic details and resolution, such as the investigation of issues associated with CNT chirality. Meanwhile, a structural molecular mechanics approach [6, 7] provides the advantage to model the "long-term" phenomenon with better computational efficiency without losing the atomistic resolution.

The structural molecular mechanics modeling technique is based on an assumption that the carbon structures in the PGS are frame-like structures, whose C-C bonds between two nearest-neighboring carbon atoms are treated as a beam element, whereas an individual atom acts as the nodal point of the related load-bearing beam members. To evaluate material and sectional properties of the hypothetical beam element, it utilizes the energy equivalence of potential energy of a covalent C-C bond from the molecular model with strain energy of a beam element from the frame-like structure of the CNT or graphite.

In our earlier study [8], we calculated 3-D stiffness properties and critical buckling loads of the PGS that consists of single-layered graphene and single-walled CNTs. In this study, we found that the single-layered PGS (sPGS) are susceptible to buckling loads because of low out-of-plane rigidity of the graphene layers compared to the rigidity of the CNT pillars. Under various modes of the compressive buckling loading, the CNT pillars hardly deform, but only cause the graphene layers to deform significantly with local bending modes. In order to enhance the structural integrity under these situations, we considered the multi-layered PGS (mPGS) that consists of multi-layers of graphene sheets (graphite) and multi-walled CNTs (MWCNTs). Note that the multi-layered graphite and the MWCNTs are more abundant and more easy to process than the single-layered graphene sheet and the single-walled CNTs.

In the current study, by using the structural molecular mechanics modeling approach, we have investigated the mechanical response of the mPGS. Computational simulations have been conducted using a finite element method for the beam-based frame structure. Results and discussions focus on 3-D effective stiffness properties of the mPGS, such as Young's and shear moduli, as well as Poisson's ratios. We compared these properties with those of the sPGS. We also conducted parametric study with various pillar lengths and inter-pillar distances to determine critical parameters for enhancing in-plane and through-thickness properties of the mPGS.

2. Simulation Methodology

We considered a two-layered mPGS in this study. The basic procedure of generating the mPGS model is similar with that for the single-layered PGS (sPGS) [8] except that the mPGS requires preparation of two different sizes of CNTs. Firstly, we need to make a hole in the middle of the graphene sheet to be fit with the CNT. In order to make an appropriate junction formation, the diameter of the hole needs to be similar with that of the CNT, and the sum of a chiral vector of the CNT, i.e., n+m, should be equal to the number of inner vertices of the graphene hole. This is required to avoid atomic vacancies or defects at the junction. The center of the hole can be located either in the center of a hexagon or in the juncture of a three-way C-C bond, which results in a 6-fold symmetry and a 3-fold symmetry, respectively. It turns out the 6-fold symmetry yields a more similar circular hole than the 3-fold symmetry, and thus we used the 6-fold symmetry in the present model. A single-walled CNT was then brought to the graphene sheet near the hole as shown in Fig.1 (a). A molecular mechanics simulation was then conducted with an AIREBO potential function to obtain an equilibrium configuration with minimal energy. The minimized configurations of two CNT-graphene junctions with (6,6) and (12,12) CNTs are shown in Fig.1 (b). These two single-layered CNT-graphene junctions can then be combined to form the multi-layered CNT-graphitic junctions, which is a basic building

block of the mPGS. Once the junction is formed, a periodic unitcell of the mPGS is formed by applying geometrical manipulations such as translation, rotation, mirror-imaging, etc. Fig.2 shows the unitcell of the mPGS and their constituents: two sPGSs and two mid-layers located between two sPGSs. The number of atoms in the present mPGS model is 9,436, and the number of C-C bonds is 13,488. The dimensions of the present mPGS are $L_x = 5.926$ nm, $L_y = 5.378$ nm and $L_z = 6.851$ nm.

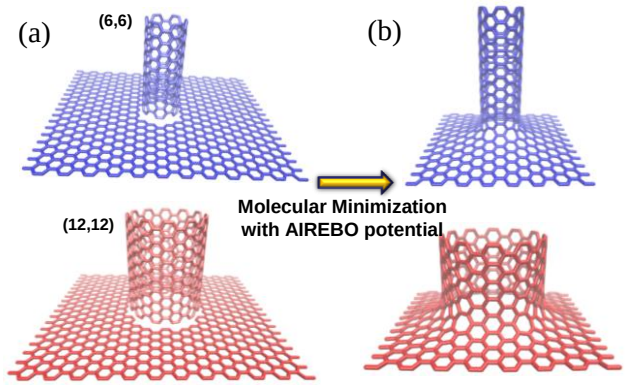

Fig.1. Development of multi-layered CNT-graphene junctions (a) before and (b) after molecular minimization with an AIREBO potential function.

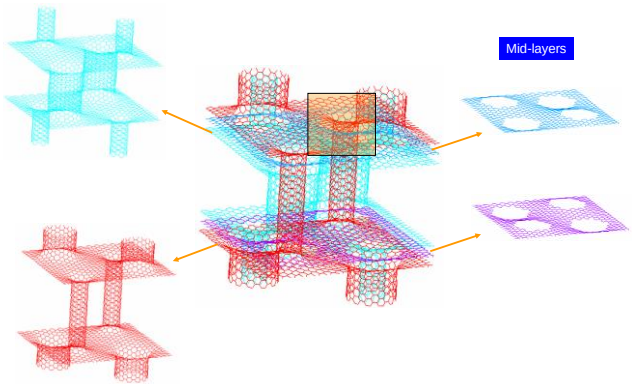

Fig.2. A unitcell of a multi-layered pillared graphene structure.

The generated mPGS unitcell atomic structures were converted into the beam finite elements for the structural molecular mechanics analysis. Proper selections of periodic boundary conditions were applied to the periodic unitcell geometry to yield consistent results on the property prediction with minimal size and edge effects.

We obtained the effective mechanical properties of the mPGS, such as Young's modulus and Poisson's ratio, in three orthogonal directions (two planar and one out-of-plane). We also generated multicell models by duplicating the aforementioned unitcell models, and calculated such mechanical properties. We found that both models yield exactly identical modulus properties when such proper periodic geometry and boundary conditions were used.

In real situations, the CNT lengths and their interval distances can change with various processing parameters. We conducted a parametric study to understand the effects of these geometric parameters on the 3-D effective properties of the mPGS. For this parametric study, we developed various periodic unitcell models for mPGSs having different values of pillar length and inter-pillar distance.

3. Simulation Results and Discussion

The 3-D effective stiffnesses of the mPGS were calculated and plotted in Fig.3. In this figure, the stiffness values of the mPGS were normalized by those of the sPGS, whose dimensions are similar with the mPGS. The dimensions of the sPGS considered here are $L_x = 5.936$ nm, $L_y = 5.384$ nm and $L_z = 6.529$ nm. Note that we neglected the VDW interactions in the present calculation since the VDW effect on the effective stiffness is relatively insignificant compared with the strong C-C bonds. As the figure shows, the mPGS composed with two sPGSs yields significantly higher Young's and shear moduli than the sPGS of the similar sizes. While the in-plane moduli (E_1, E_2 and G_{12}) are nearly proportional to the number of sPGSs, the out-of-plane Young's modulus (E_3) and shear moduli (G_{23} and G_{13}) are approximately 4.6 and 2.8 times higher than those of the sPGS, respectively. The two out-of-plane Poisson's ratios (ν_{23} and ν_{13}) of the mPGS are higher by 30% and 38%, respectively, but the in-plane Poisson's ratios (ν_{12}) is smaller by 20% than those of sPGS.

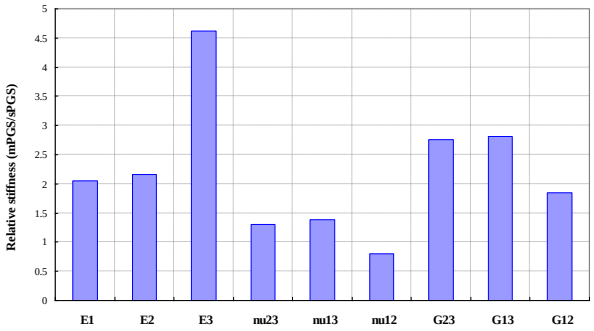

Fig.3. Ratios of effective stiffness of multi-layered PGS to single-layered PGS with similar unitcell dimensions.

For the parametric study, firstly, we considered the effect of the inter-pillar distance by increasing the unitcell length in y-direction, while fixing the other two lengths in x- and z-directions. The dimensions of the mPGS with the various y-length is plotted against the inter-pillar distance in Fig.4. Fig.5 shows 3-D Young's moduli, shear moduli and Poisson's ratios of the mPGS against the inter-pillar distance.

We found that the increase of the inter-pillar distance results in larger in-plane Young's moduli (E_1 and E_2) and smaller out-of-plane moduli (E_3). The increase of the in-plane E_1 and E_2 is attributed from less frequent CNT-graphene junctions, which possess significant curvature that affects the moduli considerably, in the planar directions. Meanwhile, the decrease of the out-of-plane E_3 is attributed from a larger cross-sectional area (A_3) that was used in the modulus calculation. We found similar trends for the shear moduli in that the increase of the inter-pillar distance results in larger in-plane shear modulus (G_{12}) and smaller out-of-plane moduli (G_{13} and G_{23}). We can also see the decreasing trend of the out-of-plane Poisson's ratios (ν_{13} and ν_{23}) with the increase of the inter-pillar distance, while the in-plane Poisson's ratio (ν_{12}) shows nearly quadratic behavior, having a minimum near 4.35 nm. Note that the in-plane ν_{12} is negative because of the curved CNT-graphene junctions. For example, when an in-plane tensile loading is applied in a direction (e.g., x-direction), the curved junctions tend to flatten in radial direction. The flattened junctions cause a positive strain in the radial direction, including an orthogonal direction to the loading (e.g, y-direction). The negative in-plane ν_{12} is then possible when this positive strain in the orthogonal direction exceeds the negative contracting strain of the graphene due to the Poisson's effect.

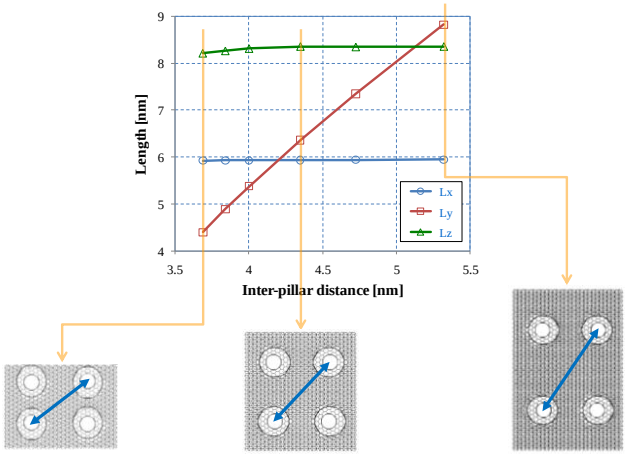

Fig.4. Dimensions of mPGS against various inter-pillar distance.

(a)

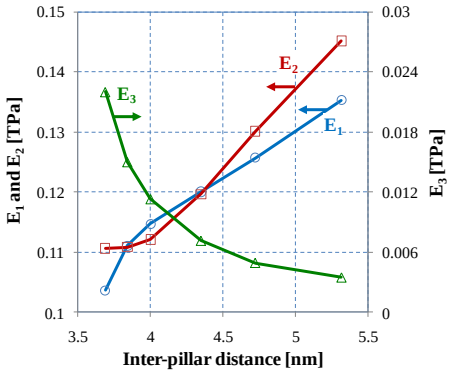

(b)

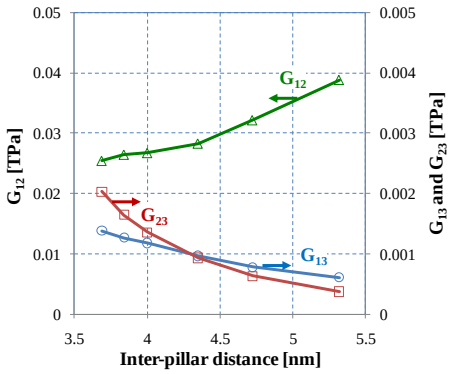

(c)

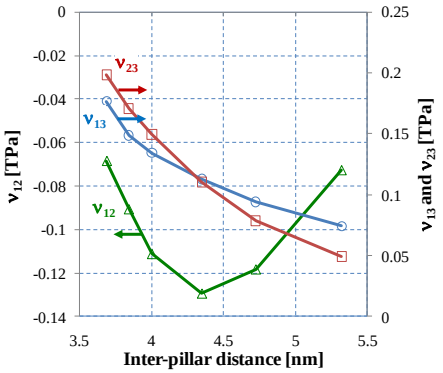

Fig.5. 3-D (a) Young's moduli, (b) shear moduli and (c) Poisson's ratios of mPGS against various inter-pillar distance.

Next, we considered the effect of the pillar length by increasing the unitcell length in z-direction, while fixing the other two lengths in x- and y-directions. The dimensions of the mPGS with the various z-length is plotted against the pillar length in Fig.6. Fig.7 shows 3-D Young's moduli, shear moduli and Poisson's ratios of the mPGS against the pillar length.

We found that the increase of the pillar length results in smaller in-plane Young's moduli (E_1 and E_2) and larger out-of-plane Young's modulus (E_3). The decrease of the in-plane E_1 and E_2 is attributed from larger cross-section areas (A_1 and A_2) that were used in the modulus calculation, while the increase of the out-of-plane E_3 is attributed from less frequent CNT-graphene junctions in the through-thickness direction. Unlike the inter-pillar distance case, all the shear moduli (G_{12} , G_{13} and G_{23}) show decreasing trends with the increase of the pillar length. As for the Poisson's ratio, we can see that the out-of-plane ν_{13} and ν_{23} increases with the increase of the pillar length, while the in-plane ν_{12} yields nearly constant values of approximately -0.093 . Note also that, regardless of the pillar length, the in-plane ν_{12} is negative because of the curved CNT-graphene junctions.

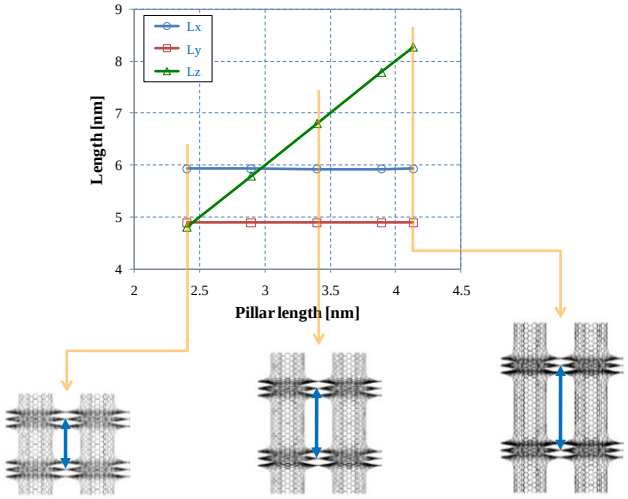

Fig.6. Dimensions of mPGS against various pillar length.

(a)

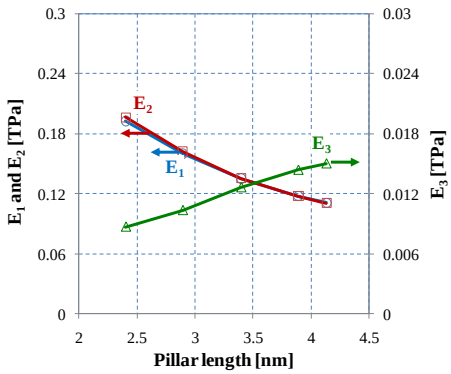

(b)

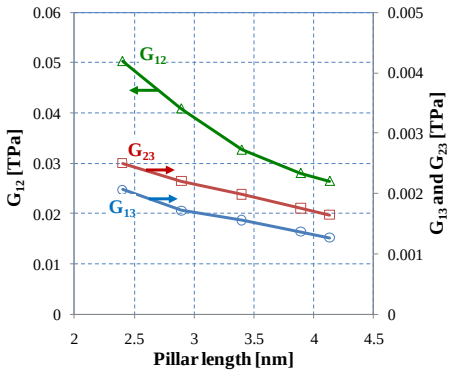

(c)

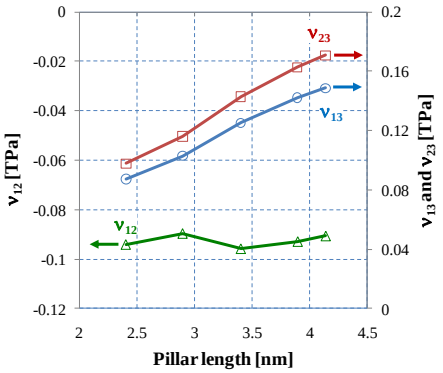

Fig.7. 3-D (a) Young's moduli, (b) shear moduli and (c) Poisson's ratios of mPGS against various pillar length.

4. Summary and Conclusions

We conducted a computational study to predict effective mechanical stiffness properties of the novel 3-D carbon structure, mPGS. We developed various periodic unitcell models for mPGSs having different values of pillar length and inter-pillar distance. These structures were converted into the beam finite elements for the structural molecular mechanics method. Proper selections of periodic boundary conditions were applied to the periodic unitcell geometry to yield consistent results on the property prediction with minimal size and edge effects.

We obtained the effective mechanical properties of the mPGS, such as Young's modulus and Poisson's ratio, in three orthogonal directions (two planar and one out-of-plane). We considered both unitcell and multicell models and found that both models yield exactly identical modulus properties when such proper periodic geometry and boundary conditions were used. The simulation results show that the mPGS yields significantly improved effective Young's and shear moduli compared with the sPGS, especially, the out-of-plane Young's and shear moduli. The parametric study carried out with the geometric variations shows that the pillar length and inter-pillar distance significantly affect the 3-D effective in-plane and through-thickness properties.

5. Acknowledgments

This work was performed under U.S. Air Force Contract No. FA8650-10-D-5011 and Air Force Office of Scientific Research.

6. References

[1] G. K. Dimitrakakis, E. Tylianakis, G. E. Froudakis "Pillared Graphene: A New 3-D Network Nanostructure for Enhanced Hydrogen Storage". *Nano Letters*, Vol. 8, No. 10, pp 3166-3170, 2008.

[2] R. K. Paul, M. Ghazinejad, M. Penchev, J. Lin, M. Ozkan, C. S. Ozkan "Synthesis of a Pillared Graphene Nanostructure: A Counterpart of Three-Dimensional Carbon Architectures". *Small*, Vol. 6, No. 20, pp 2309-2313, 2010.

[3] L. L. Zhang, Z. Xiong, X. S. Zhao "Pillaring Chemically Exfoliated Graphene Oxide with Carbon Nanotubes for Photocatalytic Degradation of Dyes under Visible Light Irradiation". *ACS Nano*, Vol., No., pp null-null, 2010.

[4] V. Varshney, S. S. Patnaik, A. K. Roy, G. Froudakis, B. L. Farmer "Modeling of Thermal Transport in Pillared-Graphene Architectures". *ACS Nano*, Vol. 4, No. 2, pp 1153-1161, 2010.

[5] F. D. Novaes, R. Rurali, P. Ordejón "Electronic Transport between Graphene Layers Covalently Connected by Carbon Nanotubes". *ACS Nano*, Vol., No., pp null-null, 2010.

[6] C. Li, T.-W. Chou "A structural mechanics approach for the analysis of carbon nanotubes". *International Journal of Solids and Structures*, Vol. 40, No. 10, pp 2487-2499, 2003.

[7] K. I. Tserpes, P. Papanikos "Finite element modeling of single-walled carbon nanotubes". *Composites Part B: Engineering*, Vol. 36, No. 5, pp 468-477, 2005.

[8] S. Sihn, V. Varshney, A. K. Roy "Modeling of Mechanical Behavior of Pillared Graphene Structures". *The 51st AIAA/ASME/ASCE/AHS/ASC Structures, Structural Dynamics, and Materials Conference*, 2010.